Optical Materials 97 (2019) 109351

Contents lists available at ScienceDirect

Optical Materials

journal homepage: www.elsevier.com/locate/optmat

Study on fluorescence characteristics of the Ho^{3+}:ZBLAN fiber under ~640 nm excitation

Meina Chen[a], Wensong Li[a,b], Shuaihao Ji[a], Xiuji Lin[a], Xuan Zhan[a], Huiying Xu[a], Zhiping Cai[a,*]

[a] Department of Electronic Engineering, Xiamen University, Xiamen, 361005, China
[b] ECE/COMSET, Clemson University, 91 Technology Drive, Anderson, SC, 29625, USA

ARTICLE INFO

Keywords:
Spectral characteristic
Ho^{3+}:ZBLAN fiber
Judd-ofelt theory
Rate equation
Visible laser

ABSTRACT

We investigated the absorption and emission characteristics of the Ho^{3+}:ZBLAN fiber under ~640 nm excitation. Based on the Judd-Ofelt theory, a detailed spectroscopic analysis on excited states $^5I_6$ and $^5I_7$ of the Ho^{3+}-ion was performed. The population dynamics was conducted by using the rate equation method, and a set of analytical expressions for population densities of various levels were obtained at steady state. Moreover, the fluorescence intensities of the $^5S_2$, $^5F_4 \rightarrow {}^5I_7$, $^5I_8$ and $^5I_6 \rightarrow {}^5I_7$, $^5I_8$ and $^5I_7 \rightarrow {}^5I_8$ transitions were measured in different pumping powers. The simulated and experimental results are quite consistent. This work could provide the spectral information for optimal design of the visible oscillations in the Ho^{3+}:ZBLAN fiber excited at ~640 nm.

1. Introduction

The ZBLAN (ZrF_4–BaF_2–LaF_3–AlF_3–NaF) glass host has a low maximum phonon energy ($< 600\ cm^{-1}$), which reduces the nonradiative transition in rare-earth ions and enables the efficient wideband lasing transitions. In the Ho^{3+}:ZBLAN fiber, the investigation of various laser oscillations ranging from the visible to mid-infrared (VIS-MIR) spectral region has been proposed. In general, an upconversion-pumped Ho^{3+}:ZBLAN fiber laser is considered for the generation of the short-wavelength visible oscillation. Allain et al. demonstrated the first tunable continuous-wave (CW) green and deep-red lasings in Ho^{3+}-doped fluoride fiber under ~647 nm Kr^+-ion laser excitation, which originates from the transitions $^5S_2$, $^5F_4 \rightarrow {}^5I_7$, $^5I_8$ of the Ho^{3+}-ion [1]. Subsequently, a set of works by Funk et al. systemically reported that the green laser oscillations (i.e. $^5S_2$, $^5F_4 \rightarrow {}^5I_8$) in the Ho^{3+}:ZBLAN fiber pumped by red laser sources, e.g. dye laser at 640–653 nm [2,3], and diode laser at ~643 nm [4,5]. Quite recently, we demonstrated a green wavelength-tunable Ho^{3+}:ZBLAN all-fiber upconversion laser using a 640 nm solid-state laser pumping [6]. However, in these works, the visible laser performance is quite poor, such as low conversion efficiency, only ~40 mW of output power at green wavelength and 2 mW at the deep-red wavelength.

Furthermore, the transitions of the Ho^{3+}-ion, including the $^5I_6 \rightarrow {}^5I_8$ at ~1.2 μm, the $^5I_7 \rightarrow {}^5I_8$ at ~2 μm, and the $^5I_6 \rightarrow {}^5I_7$ at ~2.9 μm are extensively demonstrated in the past several years. In 1992, the demonstration on the CW Ho^{3+}:ZBLAN fiber laser at 1.19 μm was first reported using ~640 nm dye laser as the pump source [7]. Recently, the broad tuning of 1177–1201 nm was realized with a bulk grating in the Ho^{3+}:ZBLAN fiber [8]. And the pulsed Ho^{3+}:ZBLAN fiber lasers operating at ~1.2 μm were also reported [9,10]. Under a blue Ar^+ laser pumping, the first lasing at 2.08 μm in the Ho^{3+}-doped fluoride fiber was proposed by Brierley et al. [11]. The wavelength tunability between 2.83 and 2.95 μm was also achieved in Ho^{3+}: ZBLAN fiber by the ~640 nm pumping [12]. Additionally, the demonstration of the dual-wavelength CW cascade oscillation at ~2 and ~3 μm was also proposed in the Ho^{3+}:ZBLAN fiber [13,14]. And the pulsed Ho^{3+}:ZBLAN fiber lasers around 3 μm were investigated [15,16].

Definitely, these above-mentioned results illustrate the wideband laser operation capability in the Ho^{3+}:ZBLAN fiber. The theoretical analysis on the lasing characteristics of the Ho^{3+}-doped fluoride glass is under investigation [17–24]. But so far, no report is proposed to reveal the spectral characteristics of the Ho^{3+}:ZBLAN fiber excited by a ~640 nm laser source [25]. Benefiting from the available high-power red-solid-state laser pumping [26], the optimization of above visible upconversion laser operation for the Ho^{3+}:ZBLAN fiber could be further implemented. In this work, we systematically discussed the emission mechanism of the Ho^{3+}-ion at ~550, ~750, ~1190, ~2060 and ~2860 nm under ~640 nm excitation. Based on the absorption spectrum, the Judd-Ofelt parameters such as spontaneous transition probabilities, transition lifetimes and fluorescence branching ratios were

* Corresponding author.
E-mail address: zpcai@xmu.edu.cn (Z. Cai).

https://doi.org/10.1016/j.optmat.2019.109351
Received 1 August 2019; Received in revised form 26 August 2019; Accepted 27 August 2019
Available online 14 September 2019
0925-3467/

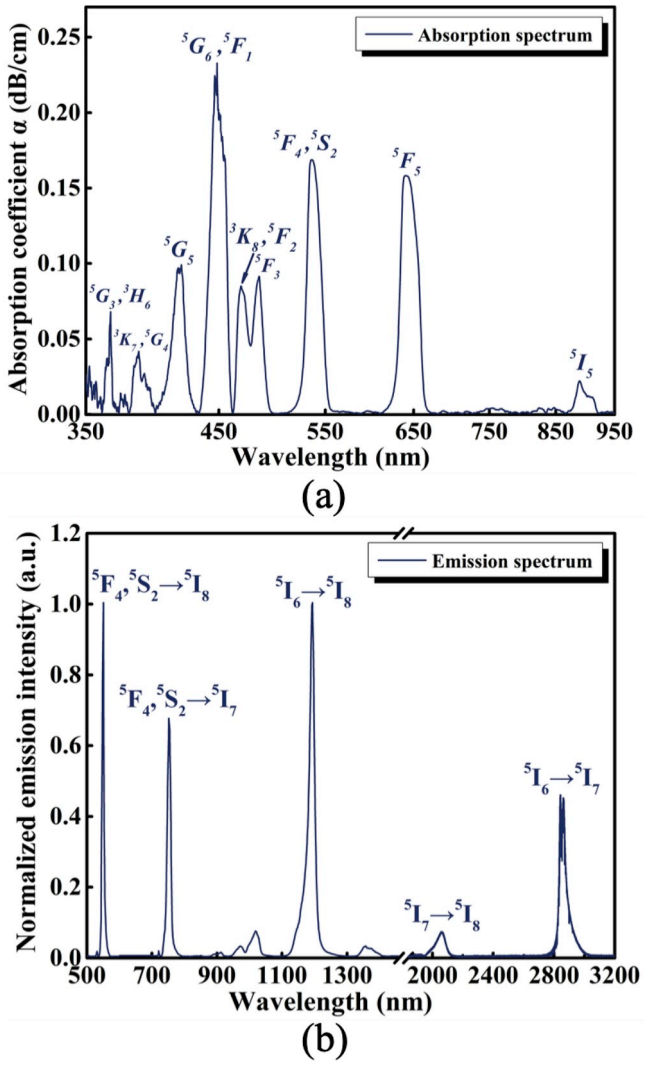

Fig. 1. (a) Absorption spectrum of 0.5 mol% Ho^{3+}: ZBLAN fiber. (b) Emission spectrum of the Ho^{3+}: ZBLAN fiber under 640 nm excitation.

calculated. By using the rate equation theory, the population dynamics of the Ho^{3+}-ion were conducted. Such a work could detailedly reveal the spectral characteristics of the Ho^{3+}:ZBLAN fiber pumped by a ~640 nm laser source, which contributes to the development of efficient visible oscillations.

2. Absorption and emission measurements

In the experiment, a 0.5 mol% Ho^{3+}:ZBLAN fiber (Le Verre Fluoré) was used with a 7.5/125 μm core/cladding diameter. We measured the VIS-NIR absorption spectrum of the Ho^{3+}:ZBLAN fiber using a HL-2000 Halogen light source (Ocean Optics). As given in Fig. 1(a), nine absorption peaks originating from the ground state corresponding to different upper states are recorded. At ~640 nm, it has a large absorption coefficient about 0.17 dB/cm.

Fig. 1(b) presents the fluorescence spectrum of the Ho^{3+}:ZBLAN fiber measured in VIS-MIR spectral range. Here the 640 nm excitation source is based on a home-made blue diode-pumped solid-state laser, as proposed in our previous works [6,26]. Limited by the available spectral range, we separately used two optical spectrum analyzers, i.e. 500–1750 nm AQ6315E (Ando) and 1 to 5.6 μm (Thorlabs 205C) to perform the emission measurement. The spectra were normalized for convenience. Obviously, the transition $^5S_2$,$^5F_4 \rightarrow {}^5I_8$ at ~550 nm and the transition $^5I_6 \rightarrow {}^5I_8$ at ~1.2 μm have the higher emission peak, indicating the stronger optical gain. A relatively lower gain is labelled at ~2.0 μm (i.e., $^5I_7 \rightarrow {}^5I_8$). The emission band around 2.86 μm (i.e., $^5I_6 \rightarrow {}^5I_7$) shows a depression due to the water absorption. The potential transitions $^5S_2$,$^5F_4 \rightarrow {}^5I_6$, $^5I_5$ at ~1.0 and ~1.3 μm respectively are not considered in this work. It should be noted that the transition $^5S_2$,$^5F_4 \rightarrow {}^5F_5$ around 3.2 μm did not be detected. All these spectroscopic behaviors will be prepared to establish the transition mechanisms in the following sections.

3. Judd-Ofelt theory calculation

Using the Judd-Ofelt (J-O) theory, we can calculate the intensity parameters Ω_λ of the Ho^{3+}:ZBLAN fiber and the spontaneous transition probability of $^5I_7$, $^5I_6$, $^5I_5$, $^5F_5$ and $^5S_2$, $^5F_4$ levels based on the absorption spectrum measured above. Parameters such as radiative lifetimes and fluorescence branching ratios allow quantitative analysis of radiation intensity to provide reliable data for subsequent calculations.

According to the J-O theory [27,28], the measured oscillator strengths and the theoretical values are fitted by the least square method. The value of $\boldsymbol{\Omega_\lambda}$ are respectively obtained: $\boldsymbol{\Omega_2 = 3.74 \times 10^{-21} cm^2}$, $\boldsymbol{\Omega_4 = 2.77 \times 10^{-20} cm^2}$, $\boldsymbol{\Omega_6 = 2.14 \times 10^{-20} cm^2}$. According to the $\boldsymbol{\Omega_{2,4,6}}$ calculated above, the value of spontaneous radiation probability $\boldsymbol{A\,(J \rightarrow J')}$, radiative lifetime $\boldsymbol{\tau_R}$ and fluorescence branch ratio $\boldsymbol{\beta\,(J \rightarrow J')}$ are calculated by the following formulas:

$$A(J \rightarrow J') = A_{ED}(J \rightarrow J') + A_{MD}(J \rightarrow J') = \frac{16\pi^3 e^2}{3\varepsilon_0 h(2J+1)\lambda^3}\left[\frac{n(n^2+2)^2}{9}S_{ED} + n^3 S_{MD}\right] \quad (1)$$

$$\tau_R = 1/\sum_{J'} A(J \rightarrow J') \quad (2)$$

$$\beta(J \rightarrow J') = \frac{A(J \rightarrow J')}{\sum_{J'} A(J \rightarrow J')} = \tau_R A(J \rightarrow J') \quad (3)$$

where A_{ED}, A_{MD}: electric dipole transition probability and magnetic dipole transition probability; S_{ED}, S_{MD}: line strength of the electric dipole and magnetic dipole transition, defined as $S_{ED} = \sum_{\lambda=2,4,6} \Omega_\lambda |\langle aJ||U^{(t)}||bJ'\rangle|^2$ and $S_{MD} = \frac{h^2}{16\pi^2 m^2 c^2} |<aJ||L + 2S||> bJ'|^2$; $|\langle aJ||U^{(t)}||bJ'\rangle|^2$: reduced matrix elements of the electronic transition from J to J' [29]. e: electron charge, m: electron mass, c: light velocity, n: the refraction index of the material, ε_0: vacuum dielectric constant, h : the Planck's constant, J: total angular momentum. The value of S_{MD} depends on the selection rule: $\Delta S = \Delta L = 0$, $\Delta J = 0, \pm 1$. The calculated values by the above formulas are listed in Table 1.

It should be mentioned that the magnitude of the nonradiative transitions from the above emitting states of the Ho^{3+}:ZBLAN fiber determines the radiative efficiency. The nonradiative rate can be further defined as the sum of W_{NR} and W_{ET}, denoting nonradiative transition and energy transfer rates, respectively. According to the Tanimura's investigation [17], for low rare-earth ion concentration $W_{ET} \cong 0$, this indicates the nonradiative transition depends on the multiphonon emission, so here we ignore the energy transfer process. Based on the literature [30], we modify the nonradiative transition formula as follows:

$$W_{NR}(T) = C \cdot \exp(-\alpha \cdot \Delta E)\left[1 - \exp\left(-\frac{h\omega}{k_B \cdot T}\right)\right]^{-\frac{\Delta E}{h\omega_{max}}} \quad (4)$$

where C and α are the positive constants characteristic of the host, equaled to $1.59 \times 10^{10}\ s^{-1}$ and 1.59×10^{-3} cm, respectively, for the ZBLAN host. ΔE is the energy difference between two neighboring levels. $\hbar\omega$ is the maximum phonon energy and ω_{max} is the maximum phonon frequency. k_B is the Boltzman constant and T is the temperature.

Table 1
Radiative properties of the Ho^{3+}:ZBLAN fiber.

Initial state J	Final state J'	λ (μm)	A_{ED} (s^{-1})	A_{MD} (s^{-1})	∑A (s^{-1})	τ_R(ms)	β(%)
$^5S_2$ ($^5F_4$)	$^5F_5$	3.22	0.4880 (2.45)	(3.90)	2366 (3846)	0.42 (0.26)	0.021 (0.17)
	$^5I_4$	2.00	41.78 (21.4)				1.77 (0.56)
	$^5I_5$	1.38	40.98 (129.5)				1.73 (3.36)
	$^5I_6$	1.02	155.6 (240.9)				6.58 (6.25)
	$^5I_7$	0.752	880.5 (345.6)				37.21 (8.97)
	$^5I_8$	0.55	1247 (3109)				52.70 (80.69)
$^5F_5$	$^5I_4$	4.45	0.038	1.21	2259.3	0.44	0.055
	$^5I_5$	2.27	7.15				0.316
	$^5I_6$	1.44	91.58				4.054
	$^5I_7$	0.95	414.55				18.35
	$^5I_8$	0.64	1744.7				77.23
$^5I_5$	$^5I_6$	3.95	5.40	4.91	156.37	6.39	6.61
	$^5I_7$	1.66	83.42				53.34
	$^5I_8$	0.89	62.64				40.06
$^5I_6$	$^5I_7$	2.86	16.67	11.02	181.09	5.52	15.30
	$^5I_8$	1.19	153.40				84.70
$^5I_7$	$^5I_8$	2.06	59.06	17.23	76.28	13.10	100

4. Characterization results and discussion

4.1. The modelling of pumping and relaxation processes

Fig. 2 shows the partial energy level diagram of a Ho^{3+}: ZBLAN fiber excited by 640 nm laser source, as well as the associated transition processes that corresponds to several fluorescence bands observed in Fig. 1(b). All the related levels are labelled using the LSJ configuration scheme.

Typically, the excited-state absorption (ESA) and the energy transfer are associated with the pumping mechanism. Here the latter is neglected. Meanwhile, the cross-relaxation process can be clearly observed while the Ho^{3+} ion concentration is increased to 1.5 mol% [20], so the cross-relaxation is ignored in this work. Based on the previous report by Piatkowski et al. [24], the magnitude of the ESA in the $^5I_6$ and $^5I_7$ levels of the Ho^{3+}-ion are close, so both of ESA process should be considered [31].

According to Table 1, the excited-state levels of the $^5I_6$ and $^5I_7$ have a longer lifetime (i.e., 5.5 ms and 13.1 ms, respectively) than that (i.e., 0.44 ms) of the excited-state level of $^5F_5$. As seen from Fig. 2, by the ground-state absorption, a 640 nm pump photon is first excited from the ground-state level $^5I_8$ to the metastable-state level $^5F_5$. It then depopulates quickly to the nearest lower metastable-state $^5I_6$ level by the nonradiative transition. The ions in $^5I_6$ level either decay to the $^5I_7$ and $^5I_8$ levels through the main radiative transition, or be brought by the pump ESA to the $^5G_5$ level, where the $^5S_2$,$^5F_4$ upper levels can be fed by the nonradiative transition. Furthermore, another similar pathway is given in Fig. 2. The pump ESA feeds the $^5F_3$ level starting from $^5I_7$ level that is fed from the $^5I_6$ level, and then the fast nonradiative relaxation feeds the $^5S_2$,$^5F_4$ upper levels. The relevant laser transitions originating from the $^5S_2$,$^5F_4$ upper levels include the wavelengths of ~550 nm, ~750 nm and ~1020 nm, respectively. In addition to the transition $^5I_6 \rightarrow {}^5I_8$ (~1190 nm), cascading of the two laser transitions of $^5I_6 \rightarrow {}^5I_7$ (~2860 nm) and $^5I_7 \rightarrow {}^5I_8$ (~2060 nm) are generated simultaneously. Under the 640 nm pumping, such relaxation processes clearly show the wideband transition of the VIS-MIR spectral region in the Ho^{3+}:ZBLAN fiber, indicating the feasibility of lasing oscillations.

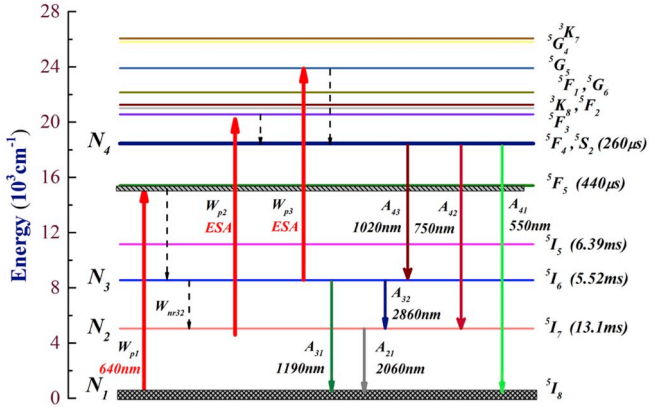

Fig. 2. Partial energy level diagram of the Ho^{3+}:ZBLAN fiber under 640 nm excitation, exhibiting the primary transition processes at the VIS-MIR wavelengths.

In order to investigate quantitatively the fluorescence intensity behavior and their relative transition mechanisms, a rate equation analysis is proposed to describe the transition dynamics of the Ho^{3+}:ZBLAN fiber under 640 nm pumping. According to the above considered energy level scheme and the relaxation processes shown in Fig. 2, a set of rate equations used to describe the dynamical behavior of the population densities $N_i(i = 1,2,3,4)$ can be written as follows:

$$\begin{aligned}
\frac{dN_1}{dt} &= -W_{p1}N_1 + A_{21}N_2 + A_{31}N_3 + A_{41}N_4 \\
\frac{dN_2}{dt} &= -(W_{p2} + A_{21})N_2 + (A_{32} + W_{nr32})N_3 + A_{42}N_4 \\
\frac{dN_3}{dt} &= W_{p1}N_1 - (A_{31} + A_{32} + W_{p3} + W_{nr32})N_3 + A_{43}N_4 \\
\frac{dN_4}{dt} &= W_{p2}N_2 - (A_{41} + A_{42} + A_{43})N_4 + W_{p3}N_3 \\
N_1 + N_2 + N_3 + N_4 &= N_t
\end{aligned} \tag{5}$$

where N_1, N_2, N_3, N_4 are the population densities of the Ho^{3+}-ion levels $^5I_8$, $^5I_7$, $^5I_6$ and $^5S_2$,$^5F_4$, respectively. N_t is the total population density of the Ho^{3+}-ion levels $^5I_8$, $^5I_7$, $^5I_6$ and $^5S_2$,$^5F_4$, and is calculated to be $6.11 \times 10^{19}\ cm^{-3}$, depending on the Ho^{3+} concentration. A_{ji} represent the radiative rate from the higher energy level j to the lower energy level i, as viewed in Table 1. W_{nr32} is the nonradiative transition rate from the $^5I_6$ level to the $^5I_7$ level, which have been calculated by Equation (4). $W_{pi}(i = 1,2,3)$ are the pumping rates from the ground-state $^5I_8$ level and from the excited-state $^5I_7$ and $^5I_6$ levels, defined as $W_{pi} = \sigma_{ai}I_{pi}/h\nu(i = 1,2,3)$, here σ_{a1}, σ_{a2}, σ_{a3} are the absorption cross sections of the ground-state $^5I_8$ level and the excited-state $^5I_7$ and $^5I_6$ levels at the 640 nm pump, respectively [24]. ν is the pump beam frequency, I_{pi} is the pump source intensity. The parameters calculated by the above formulas are as follows: $W_{nr32} = 310.27\ s^{-1}$, $\sigma_p = 5.38 \times 10^{-21}\ cm^2$, $\sigma_{esa2} = 3.81 \times 10^{-21}\ cm^2$, and $\sigma_{esa3} = 3.60 \times 10^{-21}\ cm^2$.

A steady-state solution of these equations allows to analyze the population densities. Let $\frac{dN_i}{dt} = 0$ and the steady-state solutions are given as follows:

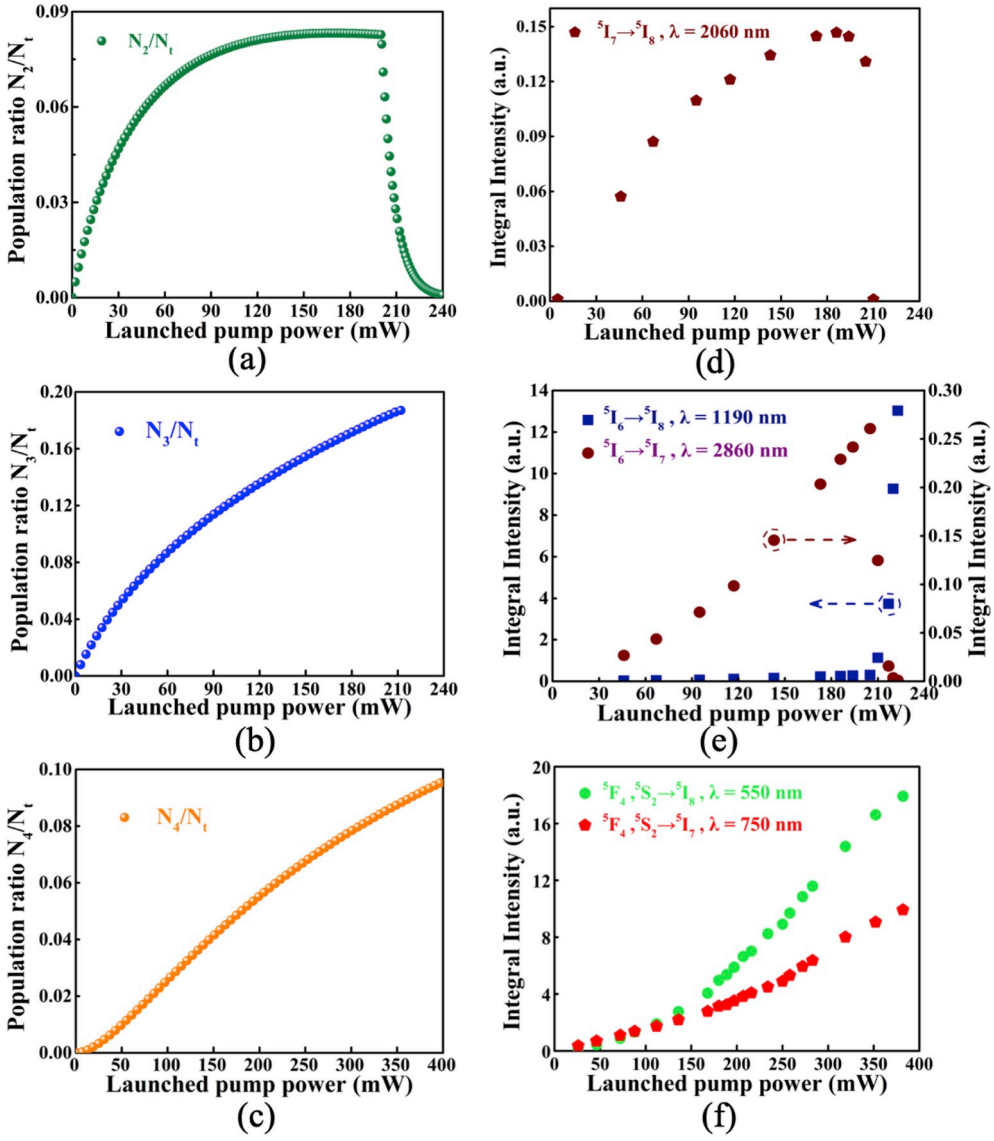

Fig. 3. Stimulated results of the population ratio versus the launched pump power. (a) N_2/N_t, (b) N_3/N_t, and (c) N_4/N_t. Experimental results of the integrated emission intensity versus the launched pump power. (d) 2060 nm, (e) 1190 nm (rectangle) and 2860 nm (circle), and (f) 550 nm (circle) and 750 nm (pentagon).

$$
\begin{aligned}
N_1 &= N_t \frac{(W_{p2} + W_{nr32} + A_3 - \gamma A_{43})}{\left[\frac{\sigma_{a2}}{\sigma_{a1}} + \gamma(1+\beta)\right] W_{p1} + (A_3 + W_{nr32} - \gamma A_{43})} \\
N_2 &= N_t \frac{(\beta\gamma - 1) w_{p1}}{\left[\frac{\sigma_{a2}}{\sigma_{a1}} + \gamma(1+\beta)\right] W_{p1} + (A_3 + W_{nr32} - \gamma A_{43})} \\
N_3 &= N_t \frac{W_{p1}}{\left[\frac{\sigma_{a2}}{\sigma_{a1}} + \gamma(1+\beta)\right] W_{p1} + (A_3 + W_{nr32} - \gamma A_{43})} \\
N_4 &= N_t \frac{\gamma W_{p1}}{\left[\frac{\sigma_{a2}}{\sigma_{a1}} + \gamma(1+\beta)\right] W_{p1} + (A_3 + W_{nr32} - \gamma A_{43})}
\end{aligned} \tag{6}
$$

where the coefficient parameters α、β and γ are defined as

$$
\alpha = \frac{A_{32} + W_{nr32}}{W_{p2} + A_{21}},\ \beta = \frac{A_{43} + A_{42} + A_{41}}{W_{p2}},\ \gamma = \frac{1+\alpha}{\beta - \frac{A_{41}}{W_{p2} + A_{21}}} \tag{7}
$$

The simulated results are shown in Fig. 3(a)-(c). It can be seen from Fig. 3(a) that the population of the $^5I_7$ level (N_2) first increases as the launched pump power increases, and then becomes saturation obviously. The population in the $^5I_6$ level (N_3) gradually increases as pump power increases as given in Fig. 3(b). Fig. 3(c) shows that the population (N_4) in the $^5S_2$,$^5F_4$ levels grows exponentially at a pump power from 0 to 150 mW, and then grows slowly.

4.2. Fluorescence intensity measurement and analysis

As given in Fig. 3(d)–(f), we also measured the evolution of the corresponding fluorescence intensity as the different pump power. For each fluorescence band, the emission intensity was calculated by integrating the emission spectrum over the available wavelength region. In Fig. 3(e), when the launched pump power is 217 mW, the self-lasing occurs first at ~1190 nm ($^5I_6$→$^5I_8$), and the emission intensity of the transition $^5I_6$→$^5I_7$ at ~2860 nm decreases rapidly and then disappears. Correspondingly, the population reduction of the $^5I_7$ level results in the disappearance of the transition $^5I_7$→$^5I_8$ at ~2060 nm, as illustrated in Fig. 3(a) and (d). Further increasing the launched pump power up to 400 mW, the emission intensities of ~550 nm ($^5S_2$, $^5F_4$→$^5I_8$) and ~750 nm ($^5S_2$, $^5F_4$→$^5I_7$) keep increasing but with saturation tendency, as presented in Fig. 3(f), which is in good agreement with Fig. 3(c). This is because the population excited to the $^5S_2$, $^5F_4$ upper levels by the ESA starting from the $^5I_6$ and $^5I_7$ levels, is gradually decreased. Interestingly, we can suppress the self-lasing of ~1190 nm ($^5I_6$→$^5I_8$) by reasonable cavity mirror design, and also the transition $^5I_6$→$^5I_7$ at ~2860 nm could be circularly oscillated within the cavity, so that the population of the $^5I_7$ level can continuously increases along with the red pumping.

Meanwhile, the population depletion of the $^5I_7$ level due to the generation of ~2060 nm ($^5I_7 \rightarrow {}^5I_8$) is stopped because of the ESA is stronger as the pumping rate enhances. Therefore, as the pump power increases, the ions in the $^5I_7$ level can incessantly populate the $^5S_2$,$^5F_4$ upper levels by the ESA to further improve the visible upconversion output.

5. Conclusion

In conclusion, the investigation on the spectral characteristics of the Ho^{3+}:ZBLAN fiber pumped by a 640 nm solid-state laser source has been performed. The J-O intensity parameters and radiative properties, such as spontaneous transition probabilities, radiative lifetimes, and fluorescence branching ratios were summarized. A numerical model employing solution of the rate equation was created with the ESA process. Moreover, we measured the emission intensities of the Ho^{3+}-ion at ~550, ~750, ~1190, ~2060, and ~2860 nm along with different pump powers. The theoretical modelling and experimental measurement of fluorescence properties in the Ho^{3+}:ZBLAN fiber are quite consistent. The objective of this work is to systematically study the spectral characteristics of the Ho^{3+}:ZBLAN fiber under 640 nm pumping, which is essential for further optimization of the visible upconversion oscillations.

Declaration of competing interest

The authors declare that they have no known competing financial interests or personal relationships that could have appeared to influence the work reported in this paper.

Acknowledgements

This work was supported by the National Natural Science Foundation of China (NSFC) (Grant No. 11674269).

References

[1] J.Y. Allain, M. Monerie, H. Poignant, Electron. Lett. 26 (1990) 261–263.
[2] D.S. Funk, S.B. Stevens, J.G. Eden, IEEE Photonics Technol. Lett. 5 (1993) 154–157.
[3] D.S. Funk, S.B. Stevens, S.S. Wu, J.G. Eden, IEEE J. Quantum Electron. 32 (1996) 638–645.
[4] D.S. Funk, J.G. Eden, J.S. Osinski, B. Lu, Electron. Lett. 33 (1997) 1958–1960.
[5] D.S. Funk, J.G. Eden, IEEE J. Quantum Electron. 37 (2001) 980–992.
[6] W.S. Li, X.F. Guan, H.Y. Xu, Z.P. Cai, OSA laser congress (ASSL), AM6A. 30 (2018).
[7] H. Többen, L. Wetenkamp, OSA Proceedings on Advanced Solid-State Lasers 13 (1992).
[8] Y.X. Ma, X.S. Zhu, L.Y. Yang, X.Z. Zhang, R.A. Norwood, N. Peyghambarian, IEEE Photonics Technol. Lett. 30 (2018) 1483–1486.
[9] X.Z. Yang, L. Zhang, X.S. Zhu, Y. Feng, Appl. Phys. B 124 (2018) 198.
[10] X.Z. Yang, L. Zhang, Y. Feng, X.S. Zhu, R.A. Norwood, N. Peyghambarian, J. Light. Technol. 34 (2016) 4266–4270.
[11] M.C. Brierley, P.W. France, C.A. Millar, Electron. Lett. 24 (1988) 539–540.
[12] L. Wetenkamp, Electron. Lett. 26 (1990) 883–884.
[13] T. Sumiyoshi, H. Sekita, Opt. Lett. 23 (1998) 1837–1839.
[14] T. Sumiyoshi, H. Sekita, T. Arai, S. Sato, M. Ishihara, M. Kikuchi, IEEE J. Sel. Top. Quantum Electron. 5 (1999) 936–943.
[15] G.W. Zhu, X.S. Zhu, K. Balakrishnan, R.A. Norwood, N. Peyghambarian, Opt. Mater. Express 3 (2013) 1365–1377.
[16] J.F. Li, H.Y. Luo, L.L. Wang, B. Zhai, H.P. Li, Y. Liu, Opt. Express 23 (2015) 22362–22370.
[17] K. Tanimura, M.D. Shinn, W.A. Sibley, M.G. Drexhage, R.N. Brown, Phys. Rev. B. 30 (1984) 2429–2437.
[18] G.F. Gan, H.X. Zheng, J. Non-Cryst. Solids 95 (1987) 771–776.
[19] L. Wetenkamp, G.F. West, H. Többen, J. Non-Cryst. Solids 140 (1992) 35–40.
[20] C.H. Qi, X.R. Zhang, H.F. Hu, Acta Opt. Sin. 14 (1994) 583–588.
[21] N. Rakov, G.S. Maciel, C.B.D. Araujo, Y. Messaddeq, J. Appl. Phys. 91 (2002) 1272–1276.
[22] A. Florez, S.L. Oliveira, M. Flórez, L.A. Gómez, L.A.O. Nunes, J. Alloy. Comp. 418 (2006) 238–242.
[23] A.F.H. Librantz, S.D. Jackson, L. Gomes, S.J.L. Ribeiro, Y. Messaddeq, J. Appl. Phys. 103 (2008) 023105.
[24] D. Piatkowski, K. Wisniewski, M. Rozanski, C. Koepke, M. Kaczkan, M. Klimczak, R. Piramidowicz, M. Malinowski, J. Phys. Condens. Matter 20 (2008) 155201.
[25] J.Y. Allaim, M.L. Flohic, M. Monerie, H. Poignant, J. Non-Cryst. Solids 161 (1993) 222–226.
[26] S.Y. Luo, X.G. Yan, Q. Cui, B. Xu, H.Y. Xu, Z.P. Cai, Opt. Commun. 380 (2016) 357–360.
[27] B.R. Judd, Phys. Rev. 127 (1962) 750.
[28] G.S. Ofelt, J. Chem. Phys. 37 (1962) 511–520.
[29] W.T. Carnall, P.R. Fields, K. Rajnak, J. Chem. Phys. 49 (1968) 4424–4442.
[30] H.W. Moos, L.A. Riseberg, Phys. Rev. 174 (1968) 429–438.
[31] M. Kowalska, G. Klocek, R. Piramidowicz, M. Malinowski, J. Alloy. Comp. 380 (2004) 156–158.